# Investigating the platinum electrode surface during Kolbe electrolysis of acetic acid

Margot Olde Nordkamp [a], Talal Ashraf [a], Marco Altomare [a], Andrea Casanova Borca [b],
Paolo Ghigna [b], Tatiana Priamushko [c], Serhiy Cherevko [c], Viktoriia A. Saveleva [d], Cesare Atzori [d],
Alessandro Minguzzi [e], Xiufang He [e], Guido Mul [a], Bastian Mei [a,f,*]

[a] *PhotoCatalytic Synthesis, Science and Technology Faculty, University of Twente, Drienerlolaan 5, 7522 NB Enschede, the Netherlands*
[b] *Dipartimento di Chimica, Università di Pavia, V.le Taramelli 13, 27100 Pavia, Italy*
[c] *Helmholtz Institute Erlangen-Nürnberg for Renewable Energy, Cauerstraße 1, 91058 Erlangen, Germany*
[d] *ESRF, The European Synchrotron, 38043 Grenoble, France*
[e] *Università degli Studi di Milano, via Golgi 19, 20133 Milano, Italy*
[f] *Technische Chemie, Ruhr-Universitität Bochum, Universitätsstraße 150, 44801 Bochum, Germany*

A R T I C L E   I N F O

A B S T R A C T

Platinum is commonly applied as the anode material for Kolbe electrolysis of carboxylic acids thanks to its superior performance. Literature claims that the formation of a barrier layer on the Pt anode in carboxylic acid electrolyte suppresses the competing oxygen evolution and promotes anodic decarboxylation. In this work, we show by using a combination of complementary *in situ* and *ex situ* surface sensitive techniques, that the presence of acetate ions also prevents the formation of a passive oxide layer on the platinum surface at high anodic potentials even in aqueous electrolyte. Furthermore, Pt dissolves actively under these conditions, challenging the technical implementation of Kolbe electrolysis. Future studies exploring the activity-structure-stability relation of Pt are required to increase the economic viability of Kolbe electrolysis.

## 1. Introduction

Today's world energy supply and chemical production processes are mainly based on fossil resources like coal, crude oil and natural gas. The environmental impact of using these resources has encouraged researchers to explore the use of green and sustainable processes to produce synthetic fuels, chemicals and building blocks [1–4]. Electrosynthesis is a means to synthesize chemical compounds by utilizing 'green' electrons supplied through solid electrodes, preferably employing the expected surplus of renewable electricity generated by wind and solar installations. Additionally, these processes are often performed at mild reaction conditions, at low pressures and temperatures.

Depending on the composition and structure of the electrocatalysts used in the electrochemical reaction, the product yield and selectivity can be tuned. To design improved electrode materials, understanding structure–activity correlations is essential and these have been determined for various electrochemical processes [5–8]. Not surprisingly, the oxygen evolution reaction (OER) is one of the most frequently studied anodic reactions [7,9–11], which is of relevance for water electrolysis, as well as in general for a broad range of electrosynthetic reactions performed in aqueous media [12–14]. Using a wide range of operando methods, such as X-ray-based techniques [15,16], isotope labeling [17], Raman spectroscopy [18] and other surface sensitive techniques including Quartz Crystal Microbalance [19], it has been demonstrated that the (electronic) structure of anodes is dynamic under OER conditions. It is thus essential to obtain detailed knowledge of the elemental composition and the crystal structure of the electrode in action [10,20, 21].

Compared to the understanding of the function of OER catalysts, significantly less is known about the structure-activity relation in electrochemical organic conversions of bio-based platform molecules, such as sugars [22], aldehydes [23] and carboxylic acids [24] .Particularly carboxylic acid conversion via Kolbe electrolysis to hydrocarbons and $CO_2$ [25], (see Figure S1 in Supporting Information) has been revisited recently. Several parameters influence the product yield and selectivity

---

of (non-)Kolbe electrolysis, such as applied current density [26], electrolyte composition [25] and electrode material [27]. Here, platinum is the electrode material of interest to facilitate radical formation. Early work of Dickinson and Wynne-Jones [28] showed that platinum electrodes are particularly suitable for Kolbe electrolysis of acetic acid, forming large quantities of ethane, whereas gold electrodes exclusively formed oxygen. Multiple explanations for the superior electrode activity of platinum exist. Most frequently, the formation of a 'barrier layer' on the surface of the platinum electrode is proposed, which supposedly inhibits the competing oxygen evolution reaction in aqueous electrolyte [29–31]. In a study of Lui et al. [29], Density Functional Theory (DFT) calculations were used to demonstrate that $CH_3COO*$ radicals strongly bind to oxidized Pt surfaces, facilitating C—C bond breaking and consecutive coupling of $CH_3*$ to ethane. Conway and Vijh [30] showed large Tafel slopes in the high potential region ($>2.1$ V), indicative for the existence of a barrier-layer type of film on the electrode. Ranninger and coworkers also studied the oxidation of acetate at moderate current densities ($< 20$ mA/cm$^2$) using Pt electrodes in methanol-based electrolyte using either LiOH and NEt$_3$ for neutralization, i.e. in the presence of low water content only [31]. They observed cathodic Pt dissolution being slightly suppressed in the presence of water, which was assigned to formation of Pt oxides. The formation of Pt oxides was later confirmed by X-ray Photon Spectroscopy (XPS) after decarboxylation of valeric acid on RuO$_2$ and Pt nanoparticles [32]. Interestingly, the cathodic dissolution rate was not dependent on electrolysis time which was assigned to the formation of an adsorbed layer of carboxylate anions. Due to the absence of such a carboxylate-barrier layer on gold and nickel electrodes, these materials are considered inactive for (non-)Kolbe electrolysis [28,33]. Despite the hypotheses on the formation of a barrier layer on Pt anodes, to date a conclusive description of the Pt surface under Kolbe conditions does not exist and the stability of Pt electrodes is not yet explored in detail particularly using aqueous electrolytes. Clearly surface sensitive experimental studies are required to fully disclose the surface structure and stability of platinum electrodes during Kolbe electrolysis.

Therefore, in this study we combine classical electrochemical techniques, such as Cyclic Voltammetry (CV) and *in situ* techniques such as electrochemical Quartz Crystal Microbalance (eQCM) and X-ray Absorption Spectroscopy (XAS), to reveal the surface structure of Pt anodes during Kolbe electrolysis of acetic acid in aqueous electrolyte. Cyclic voltammetry measurements, eQCM data and *ex situ* XAS spectra conclusively demonstrate that continuous oxidation of platinum is inhibited in the presence of acetic acid even at high current densities of 100 mA/cm$^2$ and despite the abundance of water Using Inductively Coupled Plasma Mass Spectrometry (ICP-MS) active dissolution of platinum was revealed after polarization in aqueous electrolyte at high potential. Thus, this study reveals the complex interplay between acetate ions and water leading only to a partial Pt oxide formation and active anodic Pt dissolution which in-turn inhibits the technical implementation of Kolbe electrolysis.

## 2. Experimental section

### 2.1. Materials and chemicals

Platinum foil (0.025 mm thick, 99.9 % pure, Alfa Aesar), platinized titanium mesh (Magneto Special Anodes B.V.) Pt wire (Alpha Aesar, $>99,99$ %) Ti foil, (0.5 mm thick, 99 %) were used as anode material/ support. Nitric acid (ACS reagent, 70 %), acetic acid (glacial, ReagentPlus®, $>99$ %), sodium acetate (ACS reagent, $>99.0$ %), perchloric acid (ACS reagent, 70 %), sodium perchlorate (ACS reagent $>98$ %) and PtO$_2$ ($\geq99.9$ %) all from Sigma Aldrich were used as purchased, without purification. Ultrapure water (18.2 MΩcm$^{-1}$); home made by a Millipore, Milli-Q Advantage A10 system) was used as the solvent.

### 2.2. Electrochemical measurements

All measurements were performed in a single compartment three electrode glass cell (100 ml) equipped with a platinum foil working electrode (0.8 cm$^2$ geometric area), a platinized titanium mesh counter electrode (6 cm$^2$ geometric area) and an Ag/AgCl (3 M NaCl, ProSense) reference electrode (see also Fig. S2 for a schematic of the cell), all connected to a Biologic VMP3 Potentiostat. A custom-made Teflon electrode holder was used to cover the backside of the working electrode and to have a defined exposed electrode area. Prior to each experiment the glass cell, working and counter electrode were cleaned with 10 % nitric acid and Milli-Q water to remove organic residues. The electrolyte was prepared using Milli-Q water, acetic acid and/or sodium acetate and/or perchloric acid and/or sodium perchlorate. The blank electrolyte consists of 1 M perchloric acid/sodium perchlorate and the acetic acid electrolyte consist of 1 M acetic acid/sodium acetate, with in both cases the pH adjusted to 5. After deoxygenating the freshly prepared electrolyte (70 ml) using 30 ml/min Helium ($>5.0$), the cyclic voltammograms were recorded using a scan rate of 100 mV/s. Unless mentioned otherwise, the potentials were not corrected for ohmic drop, preventing artefacts caused by overcompensation. If not stated otherwise, results are presented against the RHE scale, calculated according to the following equation:

$$E_{RHE} = E_{Ag/AgCl} + 0.059\text{pH} + E^0_{Ag/AgCl} \tag{1.1}$$

Where $E_{Ag/AgCl}$ is the measured potential and $E^0_{Ag/AgCl}$ is the Ag/AgCl (3 M NaCl) reference electrode potential ($+0.210$ V). The solution was stirred by a magnetic stirring bar, using a stirring rate of 900 rpm. All experiments were carried out at room temperature.

### 2.3. Electrochemical quartz crystal microbalance (eQCM)

EQCM experiments were performed using a Gamry eQCM 10 M at 5 MHz in a one compartment QCM cell (see Fig. S3 in the Supporting information). The sensors were Pt coated Au crystals from Q-sense (Pt film thickness of 300 nm) purchased from Quantum Design GmbH. The sensor was sandwiched between a rubber O-ring and the back contact (the exposed Pt surface area was 0.8 cm$^2$). A Pt wire was used as counter electrode and Ag/AgCl (3 M NaCl, ProSense) as reference electrode. In each experiment, 7 mL of electrolyte was used. The cell was cooled to 18 °C using a Julabo F12 water bath. Cyclic voltammetry in deoxygenated electrolyte solutions within various potential ranges was used to estimate the thickness of the PtO layer formed during Kolbe electrolysis and reference measurements. The Sauerbrey equation was used to determine the difference in mass from the shift in resonance frequency of the electrode using a calibration constant of 57 Hz cm$^2$ g$^{-1}$.

### 2.4. Inductively coupled plasma-mass spectrometry (ICP)

After polarization of the Pt foil electrode in the single compartment three electrode glass cell (described in Section 2.2), the amounts of dissolved Pt in the electrolytes were analyzed by ICP-MS (ICP-MS, PerkinElmer NexION 350 ×). ICP-MS was calibrated prior to each set of measurements by a four-point calibration slope prepared from standard solutions that contained $^{195}$Pt in a given concentration in either 0.05 M blank electrolyte (perchloric acid/sodium perchlorate) or in 0.05 M acetic acid electrolyte (acetic acid/sodium acetate). While initially both electrolyte solutions had a concentration of 1 M, the samples were diluted 20 times for the ICP-MS analysis. The dilution factor was considered during the analysis of the results. $^{187}$Re standard was used as an internal standard. The internal standard solution was prepared in 1% HNO$_3$ electrolyte and was introduced to the nebulizer of the ICP-MS via a Y-connector.

## 2.5. X-ray absorption spectroscopy (XAS)

X-ray absorption spectra were recorded at the beamline (BM-23) of the European Synchrotron Radiation Facility (ESRF) in Grenoble, France at the platinum L3-edge (11,563.7 eV). All scans were normalized with respect to the beam intensity using ATHENA. The pre-edge background was fitted by means of a straight line and the post-edge background by means of a quadratic polynomial. EXAFS data analysis was performed using the EXCURVE code using a k2 weighting scheme. To improve the signal-to-noise ratio (SNR), a spectrum was obtained by averaging 30 scans, each scan having an acquisition time of ~3 min. The XAS experiments were performed on thin film (10 nm) platinized titanium samples produced by sputtering. The reference samples, Pt foil and Pt oxide (pelletized from $PtO_2$) were measured in transmission mode to ensure optimal data quality and to avoid self-absorption. All sample measurements were performed in fluorescence mode with a low grazing incident angle of 5°. A schematic of the XAS cell is provided in Fig. S4 in the Supporting Information [34]. For *ex situ* XANES, Pt electrodes where polarized in the single compartment three electrode glass cell (described in Section 2.2),.

## 3. Results and discussion

To study the dynamics of the platinum surface under Kolbe and reference electrolyte conditions, cyclic voltammetry was used in a wide potential range (0.05–3 V vs RHE). As frequently reported, a steep increase in current, solely related to the oxygen evolution reaction, can be observed starting at ~1.7 V in the absence of acetate/acidic acid electrolyte (Fig. 1a) [25,29].

In the presence of carboxylic acids, the onset potential for oxygen evolution reaction is hardly affected, but the current density shows an inflection in the forward scan at approximately 2.2 V, resulting in a lower overall current density. This was also observed in previous literature on Kolbe oxidation of valeric acid on Pt anodes [35] and moreover our recent work confirmed the selective formation of Kolbe products at potentials > 2.2 V vs. RHE [25]. According to literature, subsequent to the formation of a stable PtO layer at potentials >1.2 V [36], a layer of deprotonated acid forms at the surface of the electrode reducing the surface coverage of $H_2O$ and $OH^-$. This results in an 'inflection zone' apparent at ~2.2 to 2.7 V, which coincides with a transition between OER at lower potentials to hydrocarbon production (Kolbe reaction) at higher potentials [29]. The formation of a platinum oxide layer and its reduction to metallic Pt can be observed for both electrolytes (Fig. 1b and c), most obviously from the oxide reduction peak minimizing at ~0.7 V for the blank electrolyte, and at ~0.6 V for the acetic acid containing electrolyte, after *prior* increase of the anodic potential to 3 V. When the voltage is limited to 1.2 V in the positive scan direction, the reduction of platinum oxide is largely suppressed. (Fig. 1b and c). A shift in the oxide reduction peak can be correlated to the thickness and

composition of the formed oxide phase, e.g. $PtO_2$ or $PtO(OH)_2$ (depending on the pH of the electrolyte) upon polarization at high potentials [37,38].

To gain further insight into the possible structure of the platinum oxide layer formed during polarization at high potentials, additional cyclic voltammetry measurements were performed. Now, *prior* to the CV scans, the Pt electrode was polarized using a constant current density of 100 mA/cm$^2$ for different durations, i.e., to pass different amounts of charge through the Pt electrode (see Figure S5 in Supporting Information for the measured potentials). After polarization, the potential was held at 1.3 V for 30 min to remove oxygen generated during polarization from the solution. After preconditioning, the formed platinum oxide film was reduced during a negative potential sweep (see Fig. S6a and b). The characteristic reduction and oxidation features of Pt seem independent of the specific treatment (Fig. S6a and b), however significant differences in the location and the area of the platinum oxide reduction peak (between 0.9 and 0.4 V vs RHE) are noticeable. The integrated charge densities of the Pt oxide reduction peak extracted from the performed CV measurements alongside with the shift in peak position relative to an unpolarized Pt anode are summarized in Fig. 2.

After polarizing the Pt anode in blank electrolyte for 12 s (until 1 C is passed), the platinum oxide reduction peak shifted by ~70 mV in the negative direction compared to the unpolarized electrode (Fig. 2a). During polarization, metallic platinum is converted to platinum oxide after which adsorbed water molecules are oxidized to oxygen gas. The slight shift of the peak potential in the negative direction and the increased area of 0.85 mC/cm$^2$ underneath the platinum oxide reduction peak after polarization are thus caused by the growth of an oxide film [39]. If the duration of polarization in blank electrolyte is increased to result in a charge accumulation of 10 C, the shape of the platinum oxide reduction peak changes from a single reduction event to a superposition of at least two contributions with an integrated charge density of 1.2 mC/cm$^2$ (See Fig. S6a in Supporting Information). Furthermore, a shift in the peak center of ~170 mV is observed. In the work of Birss et al. [37], the formation of an oxide layer of $PtO(OH)_2$ with $Pt(OH)_3HSO_4$ was reported after polarization at high anodic potentials in a 0.5 M sulfuric acid solution. Burke and coworkers also showed that platinum oxide films were formed with different compositions after anodic polarization at high potential [40,41]. As such two different forms of platinum oxides are likely observed here. Additional changes in peak area and location of the platinum oxide reduction peak after extended electrolysis were observed for even longer duration experiments and only after polarization equivalent to 150 C, the peak area and shape of the platinum oxide reduction peak resemble the structure of the sample polarized to 70 C which suggests that a steady composition of the platinum oxide film layer was obtained.

After polarizing the platinum electrode in acetic acid electrolyte (until 1 C has passed), already a shift of the platinum oxide reduction peak of ~235 mV (see Fig. 2b) was observed. The large negative shift of
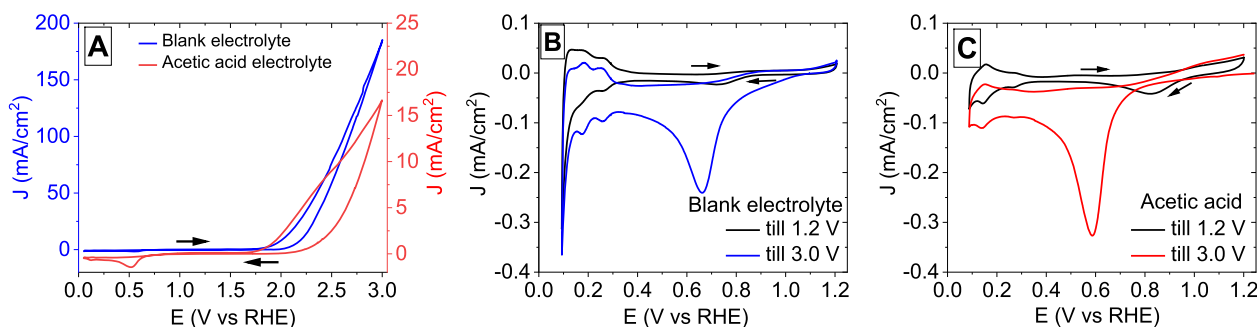


**Fig. 1.** Cyclic voltammogram of a) blank electrolyte (blue) and acetic acid electrolyte (red) in high potential window (0.05 – 3 V vs RHE) b) inset of CV in blank electrolyte c) inset of CV in acetic acid electrolyte scanned till 3 V and 1.2 V window. Scan rate: 100 mV/s. Arrows show the sweep direction. CV scans were performed in the single compartment three electrode glass cell.
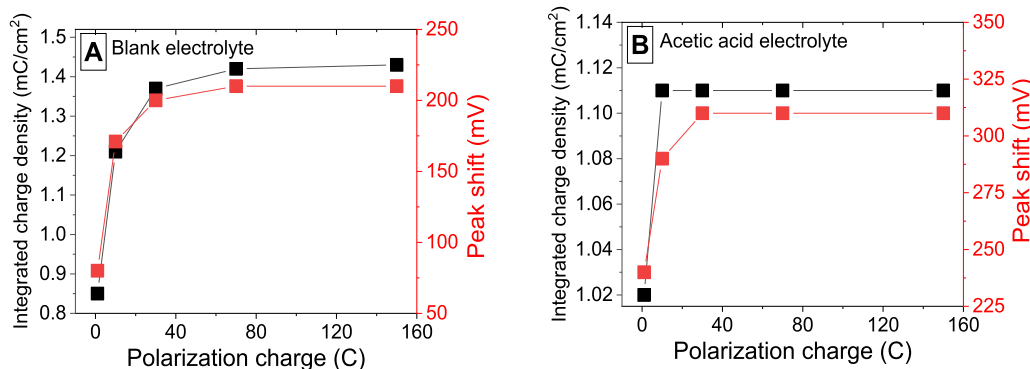
**Fig. 2.** Integrated charge density (mC/cm²) during platinum oxide reduction and the shift of the platinum oxide reduction peak to lower values (mV) relative to the unpolarized electrode after polarizing the platinum electrode at 100 mA/cm² in a) blank electrolyte and b) acetic acid electrolyte for different durations (1, 10, 30, 70 and 150 C). The solid lines are drawn to guide the eye.

the platinum oxide reduction peak is in contrast to a minor shift observed after polarization in blank electrolyte. Considering that the formation of a barrier layer is widely postulated to occur in acetic acid containing electrolytes, we assume that the extensive shift is an indication of an adsorbed $CH_3COO^-$ layer. PtO reduction is thus inhibited and requires that the formed layer on the anode desorbs, before the platinum oxide film is reduced [28,31]. At 10 C, the platinum oxide reduction peak shifts by ~310 mV relative to the unpolarized electrode, after which the position and the area of the platinum oxide reduction peak remain the same (1.11 mC/cm²) even for extended polarization (150 C). So, the polarization analysis suggests that the formation of the platinum oxide film is independent of the polarization duration once the accumulated charge is larger than 10 C.

To study the formation of the platinum oxide layer in more detail, eQCM measurements were performed to reveal the mass changes associated with platinum oxide reduction after polarization in acetic acid electrolyte. The Pt anode was pre-polarized at constant current density of 5 mA/cm² until 1, 10 or 70 C of charge were passed. The lower current density was applied to reduce the risk of electrode roughening, dissolution and delamination and thus damaging the thin Pt layer on the crystal [42,43]. Nevertheless, the relevance of the data is justified as explained in the supporting information (see Supporting Information Figs. S5 and S7). Fig. 3 displays the mass changes associated with the platinum oxide reduction (between 0.4 and 0.9 V vs. RHE typically) as a
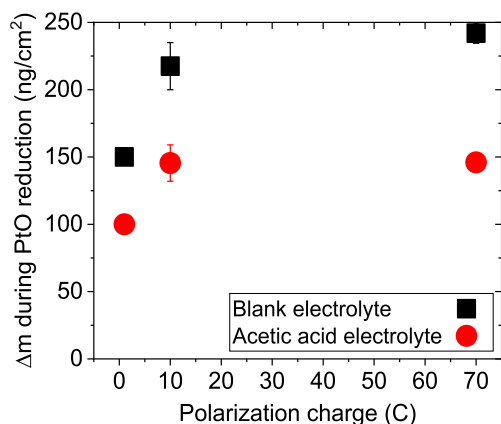
function of the polarization duration (CV scans and associated mass changes in blank and acetic acid electrolyte after polarization till 1C are shown in Fig. S8a and b in Supporting information).

It is clearly evident that the mass losses associated with the reduction of the platinum oxide layer are generally lower after polarization in acetic acid electrolyte than in blank electrolyte. This is in agreement with the overall lower integrated charge density of the platinum oxide reduction peaks obtained after polarization (Fig. 2b). For the blank electrolyte, the mass losses increase with polarization time. This indicates that the thickness of the platinum oxide layer grows as a function of polarization time, although the increase appears to stagnate with higher polarization time. This stagnation was also observed in the integrated charge density of the platinum oxide reduction peak for the blank electrolyte.

The reduction of the platinum oxide films formed after polarization to 10 C and 70 C in acetic acid electrolyte result in the same mass loss of ~145 ng/cm² (see Fig. S9a and b for reproducibility of mass loss during PtO reduction in acetic acid and blank electrolyte) being consistent with the independence of the integrated charge densities as a function of polarization time revealed by analysis of the PtO reduction signal (see Fig. 2b).

Anodic dissolution of platinum during Kolbe electrolysis was studied using Inductively Coupled Plasma Mass Spectrometry (ICP-MS). After polarization at a constant current density of 100 mA/cm² (up to 360 C), the concentration of Pt in the electrolyte was measured (see Fig. 4). Here, longer polarization durations were required to enable quantification of dissolved platinum in the electrolyte. The dissolution of Pt in acetic acid electrolyte increases linearly with polarization time whereas
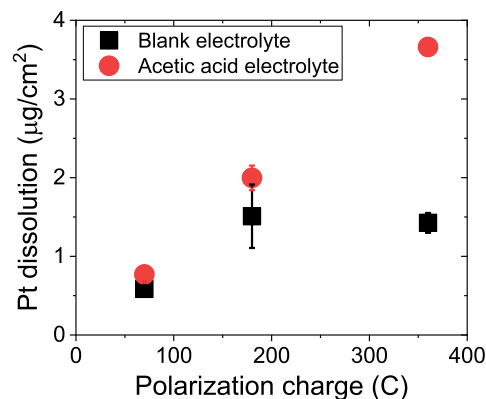


**Fig. 3.** Mass decrease (ng/cm²) during platinum oxide reduction after polarizing the platinum electrode (Pt-covered eQCM crystal with a Pt film thickness of 300 nm) at 5 mA/cm² in blank electrolyte (black squares) and acetic acid electrolyte (red circles) for different durations (1, 10 and 70) determined by eQCM. The error margins are based on $n = 2$. Note that the decrease in mass is not related to Pt dissolution but the weight loss associated with the reduction of platinum oxide to Pt. Representative raw data are shown in Fig. S8.



**Fig. 4.** Measured Pt concentration (ug/cm²) in blank (black squares) and acetic acid (red circles) electrolyte after anodic polarization of a Pt foil electrode at 100 mA/cm² for different durations (70, 180 and 360). The error margins are based on $n = 2$.

the concentration of platinum measured in blank electrolyte initially increases after which it converges to a stable value of ~1.5 μg/cm² when the polarization exceeds 180 C. Cyclic voltammetry and eQCM data discussed above suggested the formation of a barrier layer consisting of $CH_3COO^-$ anions on the electrode surface which prevents the continuous growth of platinum oxide during polarization in acetic acid electrolyte. Simultaneously, Pt complexation with dissolved acetate anions can occur [44,45], altogether enhancing the dissolution of Pt in acetic acid electrolyte leading to constant (active) Pt dissolution. In the absence of acetic acid, the continuously growing oxide layer passivates the platinum surface, resulting in decreased Pt(O) dissolution, even in aggressive media [44,46].

To complete the analysis of the PtO layer, and dissolution thereof, the electronic structure and structural changes of the platinum oxide layer were analyzed by *ex situ* X-ray absorption spectroscopy. An attempt was made to perform *in situ* X-ray absorption spectroscopy, however due to vigorous gas evolution, the obtained spectra were of poor quality (low S/N). Therefore, polarized Pt electrodes were studied *ex situ* in ambient conditions using X-ray Absorption Near Edge Structure (XANES) and Extended X-ray Absorption Fine Structure (EXAFS) spectra in fluorescence mode, after being removed from the electrolyte. Fig. 5 shows the XANES spectra obtained after polarization of the Pt anode in acetic acid electrolyte. For comparison, XANES spectra of Pt foil, $PtO_2$ reference samples, unpolarized Pt and Pt anode polarized in blank electrolyte are shown.

When comparing the XANES spectra of the unpolarized Pt electrode with the Pt foil reference spectra, the following changes can be observed: the location of the adsorption edge shifted to higher energy, the white line has a higher peak intensity and a small difference in the post-edge region is observed for the unpolarized Pt electrode. A strong white-line intensity and the dip in the post-edge region are characteristic spectral features of platinum oxides [47] (see $PtO_2$ reference spectrum in Fig. 5), this means that the unpolarized Pt electrode is slightly oxidized compared to the reference Pt foil. Possibly, a thin surface oxide film was already present after preparation of the Pt samples. After polarization in acetic acid electrolyte, no significant additional changes occur to the XANES spectra of the Pt electrode. In agreement with the previous discussion, this implies that the Pt electrode hardly oxidizes after polarization in acetic acid electrolyte. On the contrary, after polarization in blank electrolyte, the white-line peak intensity is more intense, confirming that a significantly thicker platinum oxide layer formed after polarization in blank electrolyte than in acetic acid electrolyte. This was also confirmed by linear combination fitting of the XANES spectra of the polarized anodes with the Pt foil and $PtO_2$ reference samples (see
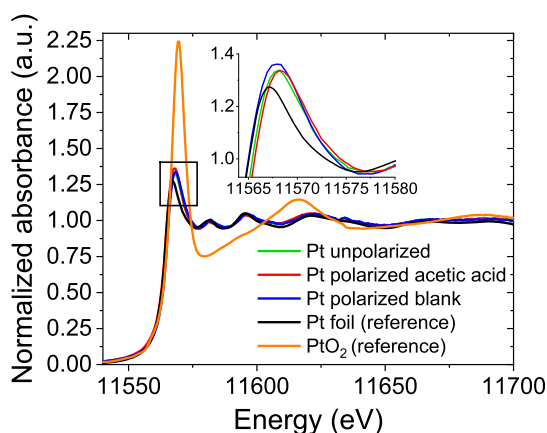
Table S2 in Supporting Information). Again, this is consistent with the presented electrochemical analysis and the eQCM data, where an overall higher mass loss during platinum oxide reduction was observed (Fig. 3). The EXAFS spectra of the polarized Pt electrodes were also recorded to investigate structural changes after polarization at high potentials, however no significant changes could be observed in the phase or amplitude of the EXAFS (See Figure S10a and 10b in Supporting Information). This suggests that the structure of the films remains unchanged after polarization and is broadly comparable to that of platinum metal. It is worthwhile noting that EXAFS analysis of the platinum oxide surface was difficult due to the low surface to bulk ratio. This should be increased for a better estimation of the structural changes.

In summary, our novel analytical data confirm that the presence of acetate (acetic acid) inhibits the formation of platinum oxide at high oxidative potentials, but stimulates significant active dissolution of Pt. In fact, data extrapolation suggests that it will take approximately 310 days until the complete Pt electrode is dissolved under continuous operation (1 cm², 0.025 mm thick, 100 mA/cm²). Thus, for technical implementation of the electrosynthesis reaction, the use of Pt needs to be reconsidered, and/or the dissolution of platinum during Kolbe electrolysis needs to be studied in more detail [31,48]. In addition, *in situ* XPS could be employed to further explore the surface structure and composition alongside with the actual oxidation state of the platinum oxide layer under Kolbe conditions.

## 4. Conclusions

Kolbe electrolysis of acetic acid on platinum anodes was investigated confirming the formation of a barrier layer of (adsorbed) acetate on the electrode surface. Particularly, it is shown that even in aqueous electrolyte and at high current densities the continuous formation of platinum oxide is suppressed. Instead under Kolbe conditions active anodic dissolution of Pt is observed. The latter has a negative impact on the practical feasibility of using Pt anodes in Kolbe electrolysis. Follow up studies to further explore the oxidation state and dissolution rate of Pt under Kolbe conditions, particularly using pulsed potential conditions or even reversed Pt polarization (using a two Pt electrodes) are required to further assess the economic viability of electro organic syntheses via Kolbe electrolysis.

## Supporting Information

The Supporting Information is available free of charge on *insert link* and contains: S1. Reaction mechanism of Kolbe electrolysis, S2 Three electrode electrochemical glass cell, S3 Gamry eQCM cell, S4 X-ray absorption spectroscopy cell, Cyclic voltammograms and potential vs. time curve of a constant current experiment in blank and acetic acid electrolyte in single compartment three electrode glass cell and eQCM reactor, S6 Cyclic voltammograms of Pt in blank and acetic acid electrolyte after polarization at high potential for different durations, S7 Relevance of the eQCM data, S8 Effect of polarization current density on the platinum oxide formation in blank electrolyte and acetic acid electrolyte, S9 CV and associated mass changes during Pt oxide reduction after polarizing the Pt anode at high potential until 1 C, S10 Reproducibility of mass changes after polarization in blank and acetic acid electrolyte, S11 EXAFS spectra of unpolarized and polarized Pt in blank and acetic acid electrolyte, S12 Linear combination fitting XANES.

## CRediT authorship contribution statement

**Margot Olde Nordkamp:** Conceptualization, Methodology, Investigation, Writing – original draft. **Talal Ashraf:** Investigation. **Marco Altomare:** Conceptualization, Methodology. **Andrea Casanova Borca:** Formal analysis. **Paolo Ghigna:** Methodology. **Tatiana Priamushko:** Investigation. **Serhiy Cherevko:** Resources. **Viktoriia A. Saveleva:** Methodology. **Cesare Atzori:** Methodology, Formal analysis.



**Fig. 5.** Pt L3-edge normalized XANES of a Pt foil reference (black), $PtO_2$ pellet reference (orange), unpolarized Pt (green), Pt after polarization in acetic acid electrolyte (red), Pt polarized in blank electrolyte (blue). The platinized titanium electrodes were polarized in acetic acid and blank electrolyte at 100 mA/cm² until 70 C of charge was reached.

**Alessandro Minguzzi:** Methodology. **Xiufang He:** Formal analysis. **Guido Mul:** Writing – review & editing, Supervision, Funding acquisition. **Bastian Mei:** Conceptualization, Methodology, Investigation, Writing – review & editing, Supervision.

## Declaration of Competing Interest

The authors declare that they have no known competing financial interests or personal relationships that could have appeared to influence the work reported in this paper.

## Data availability

Data will be made available on request.

## Supplementary materials

Supplementary material associated with this article can be found, in the online version, at doi:10.1016/j.surfin.2023.103684.

## References

[1] H. Luo, J. Barrio, N. Sunny, A. Li, L. Steier, N. Shah, I.E.L. Stephens, M.M. Titirici, Progress and perspectives in photo- and electrochemical-oxidation of biomass for sustainable chemicals and hydrogen production, Adv. Energy Mater. 11 (2021), https://doi.org/10.1002/aenm.202101180.
[2] B.A. Frontana-Uribe, R.D. Little, J.G. Ibanez, A. Palma, R. Vasquez-Medrano, Organic electrosynthesis: a promising green methodology in organic chemistry, Green Chem. 12 (2010) 2099–2119, https://doi.org/10.1039/c0gc00382d.
[3] S. Devi, N. Jyoti, N. Kiran, D. Wadhwa, J. Sindhu, Electro-organic synthesis: an environmentally benign alternative for heterocycle synthesis, Org. Biomol. Chem. 20 (2022) 5163–5229, https://doi.org/10.1039/d2ob00572g.
[4] D. Pletcher, Organic electrosynthesis – A road to greater application. A mini review, Electrochem. Commun. 88 (2018) 1–4, https://doi.org/10.1016/j.elecom.2018.01.006.
[5] O.Q. Carvalho, P. Adiga, S.K. Murthy, J.L. Fulton, O.Y. Gutiérrez, K.A. Stoerzinger, Understanding the role of surface heterogeneities in electrosynthesis reactions, IScience 23 (2020) 1–12, https://doi.org/10.1016/j.isci.2020.101814.
[6] S. Koh, J. Leisch, M.F. Toney, P. Strasser, Structure-activity-stability relationships of Pt-Co alloy electrocatalysts in gas-diffusion electrode layers, J. Phys. Chem. C 111 (2007) 3744–3752, https://doi.org/10.1021/jp067269a.
[7] R.V. Mom, L.J. Falling, O. Kasian, G. Algara-Siller, D. Teschner, R.H. Crabtree, A. Knop-Gericke, K.J.J. Mayrhofer, J.J. Velasco-Vélez, T.E. Jones, Operando structure-activity-stability relationship of iridium oxides during the oxygen evolution reaction, ACS Catal. 12 (2022) 5174–5184, https://doi.org/10.1021/acscatal.1c05951.
[8] C.L. Bentley, M. Kang, P.R. Unwin, Nanoscale surface structure-activity in electrochemistry and electrocatalysis, J. Am. Chem. Soc. 141 (2019) 2179–2193, https://doi.org/10.1021/jacs.8b09828.
[9] S. Mezzavilla, C. Baldizzone, A.C. Swertz, N. Hodnik, E. Pizzutilo, G. Polymeros, G.P. Keeley, J. Knossalla, M. Heggen, K.J.J. Mayrhofer, F. Schüth, Structure-activity-stability relationships for space-confined PtxNiy nanoparticles in the oxygen reduction reaction, ACS Catal. 6 (2016) 8058–8068, https://doi.org/10.1021/acscatal.6b02221.
[10] N. Danilovic, R. Subbaraman, K.C. Chang, S.H. Chang, Y.J. Kang, J. Snyder, A.P. Paulikas, D. Strmcnik, Y.T. Kim, D. Myers, V.R. Stamenkovic, N.M. Markovic, Activity-stability trends for the oxygen evolution reaction on monometallic oxides in acidic environments, J. Phys. Chem. Lett. 5 (2014) 2474–2478, https://doi.org/10.1021/jz501061n.
[11] R. Li, B. Hu, T. Yu, H. Chen, Y. Wang, S. Song, Insights into correlation among surface-structure-activity of cobalt-derived pre-catalyst for oxygen evolution reaction, Adv. Sci. 7 (2020), https://doi.org/10.1002/advs.201902830.
[12] M. Klein, S. Waldvogel, Counter electrode reactions — important stumbling blocks on the way to a working electro-organic synthesis, Angew. Chem. - Int. Ed. 61 (2022) 1–17, https://doi.org/10.1002/anie.202204140.
[13] S. Park, D. Thasia Wijaya, J. Na, C.W. Lee, Towards the large-scale electrochemical reduction of carbon dioxide, Catalysts 11 (2021) 253, https://doi.org/10.3390/catal11020253.
[14] J. Yoshida, K. Kataoka, R. Horcajada, A. Nagaki, Modern strategies in electroorganic synthesis, Chem. Rev. 108 (2008) 2265–2299, https://doi.org/10.1021/cr0680843.
[15] L.J. Frevel, R. Mom, J.J. Velasco-Vélez, M. Plodinec, A. Knop-Gericke, R. Schlögl, T.E. Jones, In situ X-ray spectroscopy of the electrochemical development of iridium nanoparticles in confined electrolyte, J. Phys. Chem. C 123 (2019) 9146–9152, https://doi.org/10.1021/acs.jpcc.9b00731.
[16] A. Minguzzi, O. Lugaresi, E. Achilli, C. Locatelli, A. Vertova, P. Ghigna, S. Rondinini, Observing the oxidation state turnover in heterogeneous iridium-based water oxidation catalysts, Chem. Sci. 5 (2014) 3591–3597, https://doi.org/10.1039/c4sc00975d.
[17] K.A. Stoerzinger, O. Diaz-Morales, M. Kolb, R.R. Rao, R. Frydendal, L. Qiao, X.R. Wang, N.B. Halck, J. Rossmeisl, H.A. Hansen, T. Vegge, I.E.L. Stephens, M.T.M. Koper, Y. Shao-Horn, Orientation-dependent oxygen evolution on RuO2 without lattice exchange, ACS Energy Lett. 2 (2017) 876–881, https://doi.org/10.1021/acsenergylett.7b00135.
[18] Y. Deng, A.D. Handoko, Y. Du, S. Xi, B.S. Yeo, In situ Raman spectroscopy of copper and copper oxide surfaces during electrochemical oxygen evolution reaction: identification of CuIII oxides as catalytically active species, ACS Catal. 6 (2016) 2473–2481, https://doi.org/10.1021/acscatal.6b00205.
[19] R. Frydendal, E.A. Paoli, B.P. Knudsen, B. Wickman, P. Malacrida, I.E.L. Stephens, I. Chorkendorff, Benchmarking the stability of oxygen evolution reaction catalysts: the importance of monitoring mass losses, ChemElectroChem 1 (2014) 2075–2081, https://doi.org/10.1002/celc.201402262.
[20] S. Cherevko, A.R. Zeradjanin, A.A. Topalov, N. Kulyk, I. Katsounaros, K.J.J. Mayrhofer, Dissolution of noble metals during oxygen evolution in acidic media, ChemCatChem 6 (2014) 2219–2223, https://doi.org/10.1002/cctc.201402194.
[21] S. Cherevko, S. Geiger, O. Kasian, N. Kulyk, J.P. Grote, A. Savan, B.R. Shrestha, S. Merzlikin, B. Breitbach, A. Ludwig, K.J.J. Mayrhofer, Oxygen and hydrogen evolution reactions on Ru, RuO2, Ir, and IrO2 thin film electrodes in acidic and alkaline electrolytes: a comparative study on activity and stability, Catal. Today 262 (2016) 170–180, https://doi.org/10.1016/j.cattod.2015.08.014.
[22] S. Hebié, L. Cornu, T.W. Napporn, J. Rousseau, B.K. Kokoh, Insight on the surface structure effect of free gold nanorods on glucose electrooxidation, J. Phys. Chem. C 117 (2013) 9872–9880, https://doi.org/10.1021/jp401009r.
[23] C.J. Bondue, F. Calle-Vallejo, M.C. Figueiredo, M.T.M. Koper, Structural principles to steer the selectivity of the electrocatalytic reduction of aliphatic ketones on platinum, Nat. Catal. 2 (2019) 243–250, https://doi.org/10.1038/s41929-019-0229-3.
[24] G. Yuan, C. Wu, G. Zeng, X. Niu, G. Shen, L. Wang, X. Zhang, R. Luque, Q. Wang, Kolbe electrolysis of biomass-derived fatty acids over Pt nanocrystals in an electrochemical cell, ChemCatChem 12 (2020) 642–648, https://doi.org/10.1002/cctc.201901443.
[25] M.O. Nordkamp, B. Mei, R. Venderbosch, G. Mul, Study on the effect of electrolyte ph during Kolbe electrolysis of acetic acid on Pt anodes, ChemCatChem 14 (2022), https://doi.org/10.1002/cctc.202200438.
[26] H.-J. Schäfer, Recent contributions of kolbe electrolysis to organic synthesis, Electrochem. IV (2005) 91–151, https://doi.org/10.1007/bfb0034365.
[27] T. Ashraf, A. Paradelo Rodriguez, B.T. Mei, G. Mul, Electrochemical decarboxylation of acetic acid on boron-doped diamond and platinum functionalised electrodes for pyrolysis-oil treatment, Faraday Discuss. 247 (2023) 254–269.
[28] T. Dickinson, W. Wynne-Jones, Mechanism of Kolbe's electrosynthesis, Trans. Faraday Soc. 58 (1961) 382–387.
[29] S. Liu, N. Govindarajan, H. Prats, K. Chan, Understanding the reaction mechanism of Kolbe electrolysis on Pt anodes Chem Catal. 2 1–28.
[30] B.E. Conway, A.K. Vijh, Controlled potential studies on the Kolbe reaction and the role of coadsorbed surface oxides. I. Platinum in trifluoroacetate solutions, J. Phys. Chem. 71 (1967) 3637–3654, https://doi.org/10.1021/j100870a046.
[31] J. Ranninger, P. Nikolaienko, K.J.J. Mayrhofer, B.B. Berkes, On-line electrode dissolution monitoring during organic electrosynthesis: direct evidence of electrode dissolution during Kolbe electrolysis, ChemSusChem 15 (2022) 1–7, https://doi.org/10.1002/cssc.202102228.
[32] Y. Qiu, J.A. Lopez-Ruiz, G. Zhu, M.H. Engelhard, O.Y. Gutiérrez, J.D. Holladay, Electrocatalytic decarboxylation of carboxylic acids over RuO2 and Pt nanoparticles, Appl. Catal. B Environ. 305 (2022) 0–1, https://doi.org/10.1016/j.apcatb.2021.121060.
[33] I. Sekine, H. Ohkawa, An analysis of impedance in the Kolbe reaction on platinum and gold anodes in aqueous acetate solutions, Bull. Chem. Soc. Jpn. 52 (1979) 2853–2857, https://doi.org/10.1246/bcsj.52.2853.
[34] M.L. Foresti, A. Pozzi, M. Innocenti, G. Pezzatini, F. Loglio, E. Salvietti, A. Giusti, F. D'Anca, R. Felici, F. Borgatti, In situ X-ray analysis under controlled potential conditions: an innovative setup and its application to the investigation of ultrathin films electrodeposited on Ag(1 1 1), Electrochim. Acta 51 (2006) 5532–5539, https://doi.org/10.1016/j.electacta.2006.02.031.

[35] Y. Qiu, J.A. Lopez-Ruiz, U. Sanyal, E. Andrews, O.Y. Gutiérrez, J.D. Holladay, Anodic electrocatalytic conversion of carboxylic acids on thin films of $RuO_2$, $IrO_2$, and Pt, Appl. Catal. B Environ. 277 (2020), https://doi.org/10.1016/j. apcatb.2020.119277.

[36] Y. Furuya, T. Mashio, A. Ohma, N. Dale, K. Oshihara, G. Jerkiewicz, Surface oxide growth on platinum electrode in aqueous trifluoromethanesulfonic acid, J. Chem. Phys. 141 (2014), https://doi.org/10.1063/1.4898707.

[37] V.I. Birss, M. Chang, J. Segal, Platinum oxide film formation-reduction: an in-situ mass measurement study, J. Electroanal. Chem. 355 (1993) 181–191, https://doi. org/10.1016/0022-0728(93)80361-K.

[38] A.E. Russell, Electrocatalysis: theory and experiment at the interface, Phys. Chem. Chem. Phys. 10 (2008) 3607–3608, https://doi.org/10.1039/b808799g.

[39] C.F. Zinola, A.M. Castro Luna, W.E. Triaca, A.J. Arvia, Electroreduction of molecular oxygen on preferentially oriented platinum electrodes in acid solution, J. Appl. Electrochem. 24 (1994) 119–125, https://doi.org/10.1007/BF00247782.

[40] L.D. Burke, M.M. Murphy, Effect of solution pH on hydrous oxide growth and reduction on polycrystalline platinum, J. Electroanal. Chem. 305 (1991) 301–312.

[41] L.D. Burke, J.F. O'sullivan, The stability of hydrous oxide films on platinum, J. Appl. Electrochem. 21 (1991) 151–157.

[42] Y. Sugawara, A.P. Yadav, A. Nishikata, T. Tsuru, Electrochemical quartz crystal microbalance study on dissolution of platinum in acid solutions, Electrochemistry 4 (2006) 359–365, https://doi.org/10.5796/electrochemistry.75.359.

[43] T. Sakura, T. Shibata, M. Horiuchi, R. Yagi, I. Kondo, Study of platinum dissolution mechanism using a highly sensitive electrochemical quartz crystal microbalance, Chem. Lett. 40 (2011) 402–404, https://doi.org/10.1246/cl.2011.402.

[44] Y.M. Kolotyrkin, V.V. Losev, A.N. Chemodanov, Relationship between corrosion processes and oxygen evolution on anodes made from noble metals and related metal oxide anodes, Mater. Chem. Phys. 19 (1988) 1–95, https://doi.org/10.1016/ 0254-0584(88)90002-8.

[45] Z. Wang, E. Tada, A. Nishikata, In situ analysis of chloride effect on platinum dissolution by a channel-flow multi-electrode system, J. Electrochem. Soc. 161 (2014) F845–F849, https://doi.org/10.1149/2.0431409jes.

[46] S. Cherevko, A.A. Topalov, A.R. Zeradjanin, G.P. Keeley, K.J.J. Mayrhofer, Temperature-dependent dissolution of polycrystalline platinum in sulfuric acid electrolyte, Electrocatalysis 5 (2014) 235–240, https://doi.org/10.1007/s12678- 014-0187-0.

[47] D. Friebel, D.J. Miller, C.P.O. Grady, T. Anniyev, J. Bargar, H. Ogasawara, T. Wikfeldt, L.G.M. Pettersson, In situ x-ray probing reveals fingerprints of surface platinum, Phys. Chem. Chem. Phys. 13 (2011) 262–266.

[48] K. Neubert, M. Schmidt, F. Harnisch, Platinized titanium as alternative cost-effective anode for efficient kolbe electrolysis in aqueous electrolyte solutions, ChemSusChem 14 (2021) 3097–3109, https://doi.org/10.1002/cssc.202100854.